



Synthesis and characterization of ZnO-functionalized multiwall carbon nanotubes nanocomposite as NO_x gas sensor

Pooya Gholami^{1,2} · Alimorad Rashidi² · Masoud Khaleghi Abbasabadi² · Mahnaz Pourkhalil² · Mansour Jahangiri¹ · Nosrat Izadi²

Received: 27 January 2020 / Accepted: 19 May 2020 / Published online: 27 May 2020
© Springer Nature B.V. 2020

Abstract

Synthesis of nano-zinc oxide-oxidized multiwall carbon nanotubes (ZnO-OMWCNTs) nanocomposite with different weight percentages of OMWCNTs via a multistep procedure has been described. The structure of this newly synthesized ZnO-OMWCNT was fully characterized by X-ray diffraction, scanning electron microscopy, Raman spectroscopy, and Fourier-transform infrared (FT-IR) techniques. In this research, nano-ZnO-OMWCNTs with different weight percentages of oxidized multiwall carbon nanotubes ($X=0, 0.1, 0.5, 1, \text{ and } 2 \text{ wt}\%$) were prepared. Alumina substrate with gold electrodes was labeled by sputtering, and then, the nanocomposite was deposited using spin coating machine. The sensor efficiency of nano-ZnO-OMWCNTs as recyclable nanosensor was explored in probe of nitrous oxide (NO_x) gas at the concentration of 20–40 ppm NO_x and evaluated at different temperatures (150–300 °C). Detection of NO_x gas by ZnO-OMWCNTs sensor was studied under different experimental conditions, and the results were compared by previous studies with ZnO and another metal oxide. The results show that the responsiveness, detection range, and optimum temperature of ZnO-OMWCNTs sensor performance at 250 °C were improved compared to other works. Also, adding 1 wt% of multiwall carbon nanotubes functionalized (FMWCNT) leads to an increase in sensitivity and reduces the operating temperature to 150 °C.

Keywords Oxidized multiwall carbon nanotubes · Nanosensors · NO_x · Pollutants · Zinc oxide

✉ Masoud Khaleghi Abbasabadi
Masoudkhaleghiabbasabadi@gmail.com

¹ Faculty of Chemical, Petroleum and Gas Eng, Semnan University, P.O. Box 35196-45399, Semnan, Iran

² Nano Technology Center, Research Institute of Petroleum Industry (RIPI), P.O. Box 14665-1998, Tehran, Iran

Introduction

Due to inappropriate use of fossil fuels, large amounts of toxic gases, such as CO_x , SO_2 and NO_x , release to the atmosphere every year. The most well-known pollutant among the above gases is NO_x that has huge impact on both human being and environment. To achieve a suitable solution for eliminating these kinds of pollutants, identifying the exact type of contaminants is the most important object [1–3].

In recent years, nanostructured carbon materials have received considerable attention due to their capability for utilizing in various fields such as environment, water, chemical reaction, energy, and biomedicine. Moreover, nanostructured carbon materials have found wide applications as a sensor for gas sensing owing to their interesting features such as high efficiency, environmental compatibility, corrosion resistance, air stability, low energy consumption, and low cost [4–13]. These features make them superior over other nanosensors. Other studies have shown that carbon-based nanoadsorbents, such as functionalized carbon nanotubes (CNTs), are very effective as a NO_x sensor [14]. Collins et al. [15] have demonstrated that CNTs exhibit very good adsorption properties, since they have high specific surface areas, nanoscale structures, and large number of sites. CNTs electric properties are altered by adsorption of gaseous molecules onto their surface and act as gas sensors [16].

Nanomaterials have been extensively studied for various applications in several fields including chemical industry, medical diagnostics, food technology, and ultraviolet testing [17–20]. Among nanomaterials, ZnO , SnO_2 , TiO_2 , and ZnS semiconductor nanomaterials received most attentions due to their fascinating nanosize effects which affect their physical and chemical properties [21, 22]. To make functional devices, ZnO nanostructures are promised candidates because of their low toxicity, thermal stability, oxidation resistibility, biocompatibility, large specific surface area, and high electron mobility [23]. With a direct band gap ($E_g = 3.37$ eV), large exciton binding energy (60 meV), and displaying near UV emission, ZnO is a transparent semiconductor [24–26].

The synthesis of novel nanocomposites using nanostructured carbon materials with developed advanced properties has shown excessive attention. The fabrication of CNT-based nanocomposites with various polymers, biomolecules, organic molecules, and metallic nanoparticles has been made to discover upcoming applications. These CNT-based nanocomposites have several important applications in chemical sensors, biological systems, and energy storage devices [27–29]. Previously, combination of CNT and ZnO has been reported to improve the sensing properties [30–34]. Herein, we would like to report the preparation of a new ZnO -functionalized multiwall carbon nanotubes nanocomposite employing it as a NO_x sensor for the first time. The aims of this research are: (1) to characterize the structural and chemical properties of the newly synthesized ZnO -functionalized multiwall carbon nanotubes and (2) to examine whether the functionalization on the basis of MWCNTs and hybrid with nano- ZnO can enhance the performance for NO_x sensor. According to the gain results (with the target gas concentration of

20–40 ppm), ZnO-functionalized multiwall carbon nanotubes nanocomposite can be used as a NO_x gas sensor at low concentrations with high efficiency. This study is reported for the first time in this research.

Experimental

General

All chemicals were obtained from Merck company (unless noted ones). Ultrasonication was performed in a 2200 ETH-SONICA ultrasound cleaner with a frequency of 45 kHz. Fourier-transform infrared (FT-IR) spectra were recorded from KBr pellets using a Shimadzu-8400S Spectrometer. Scanning electron microscopy (SEM) images were obtained using a VEGA TESCAN microscope with an accelerating voltage of 30.00 kV. PH of the samples was measured with a PH meter model Metrohm 744. Powder X-ray diffraction (XRD) was conducted on a Philips pw-1840 with monochromatized X-ray diffractometer. Spin coating technique was done by using a spin coater model MLW-T5. Raman spectra were recorded using a HORIBA Explora spectrometer.

Preparation of multiwall carbon nanotubes (MWCNTs)

Multiwall carbon nanotubes (MWCNTs) were prepared by chemical vapor deposition (CVD) method in a fluidized bed reactor under the flow of CH_4 and H_2 gases in which Co–Mo/MgO was used as a nanocatalyst [35].

Preparation of oxidized multiwall carbon nanotubes (OMWCNTs)

MWCNTs were oxidized using a mixture of $\text{HNO}_3/\text{H}_2\text{SO}_4$ (ratio 1/3), as previously described [4, 36]. The oxidation reaction was performed by adding about 5 g of MWCNTs to a mixture of 400 ml acid (mixture of $\text{HNO}_3/\text{H}_2\text{SO}_4$ (ratio 1/3)). Then, the solution was sonicated for 3 h at 60 °C. After sonication, the contents of the paper were filtered and washed with distilled water, while it will reach the pH of about 1.5 to 7. Finally, the resulting black solid was then dried under an oven at 80 °C for 12 h to obtain OMWCNTs [37].

Preparation of ZnO-OMWCNTs nanocomposite

ZnO-OMWCNTs nanocomposites were synthesized using a simple sol–gel method based on Zhu's work [38]. First, 5.5 gr of zinc acetate was dissolved in 1.25 L DEG. Then, 50 mL of DI H_2O was added into the above solution. Afterward, the mixture was stirred at 170 °C for 10 min and placed in air for 2 h to form aged homogeneous ZnO sol. At this step, the resulting cell was divided into five sections and each placed in a separate container. In the second step, the amount of purified OMWCNTs was dispersed into the above sol for 30 min. After that, the solution was heated

to 170 °C with vigorous magnetic stirring for 2 h. Finally, being cooled to the room temperature, ZnO-OMWCNTs nanocomposites were obtained after centrifuging, washing by EtOH and DI H₂O three times, and drying at 80 °C for 24 h [15]. For comparison, pure ZnO was prepared via sol method under the same conditions. The codes of the composite samples are listed in Table 1. The substrates were washed with deionized H₂O and then placed in a solution of EtOH for 10 min in an ultrasonic, and then, samples were placed in an oven to dry.

Electrodes investment

By using sputtering device with a height of 300 mm and a distance of 3 mm, gold particles were deposited on a substrate. During this process, gold acts as an electrode.

Deposition

The 0.2 gr of the synthesized material in 3 ml of ethanol was placed for 1 h in an ultrasonic. The material was deposited on alumina with spin coating machine with speed of 600 rpm. Then, it was heated for 2 h at 400 °C under a nitrogen atmosphere (to gain a good adhesion between the substrate and delicate matter). During this process, remained DEG was completely removed from sample. After the deposition, prepared alumina substrate was placed in the holder and connected by silver paste. Then, it was heated for 2 h in a 200 °C oven.

Gas detection setup

A schematic of the gas detection setup is shown in Fig. 1. The gas detection equipment consists of gas suppliers, mass flow controllers, a detector, a U-like quartz glass reactor (diameter of 2.5 cm and a length of about 150 cm), a jacket heater, and GAS4 software which were used for a data acquisition. The temperature was measured by a J-type thermocouple, and setpoint was controlled by a DC power supply system. The output DC voltage from thermocouple was monitored by a digital thermometer. The DC electrical conductance of the sensors during the gas exposures has been measured by the volt-amperometric technique in the two-pole format by an additional multimeter. The fabricated sensor was inserted in the glass reactor

Table 1 Code of the composites

Number	Sample name	Sample code
1	ZnO	ZnO
2	0.1 wt% ZnO-OMWCNTs	Z-MW-1
3	0.5 wt% ZnO-OMWCNTs	Z-MW-2
4	1 wt% ZnO-OMWCNTs	Z-MW-3
5	2 wt% ZnO-OMWCNTs	Z-MW-4

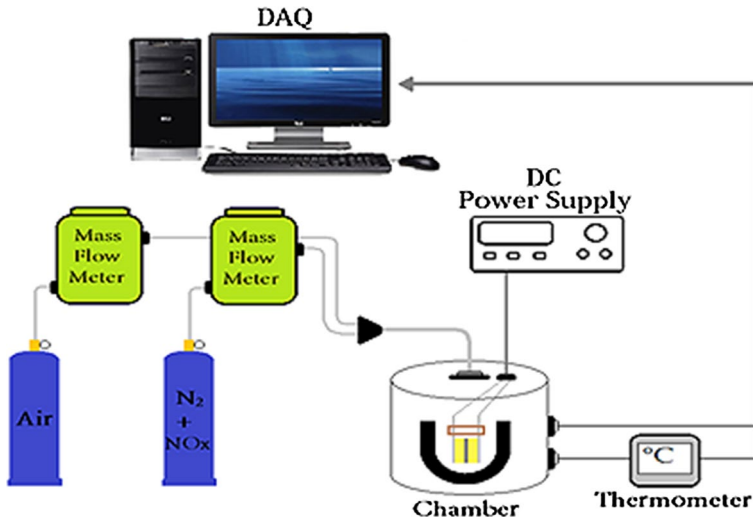


Fig. 1 Experimental setup used for gas sensing measurements of the chemiresistors

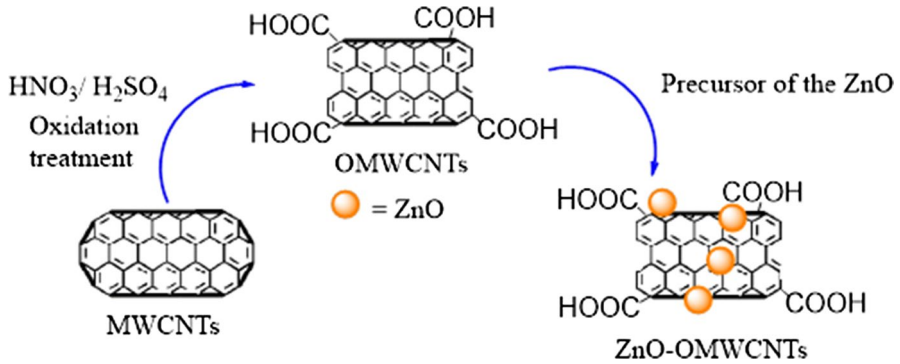
and connected to the measurement unit by wires to record the variation of electrical conductance of the sensitive films versus time. Dry air and NO_x (in mixture with nitrogen) were used as reference and detecting gases, respectively. The gas sensing experiments have been performed at temperature of 150 °C up to 300 °C, and the total flow rate of NO_x and carrier dry air per exposure was kept constant at 20–40 ppm. The concentrations of NO_x gas were controlled by mass flow meters and regulated by diluting dry air through the mixer. The initial resistance (R_{air}) was measured in dry air at test temperature. The sensitivity of the nanosensors was calculated as the ratio of the change in its electrical resistance with NO_x to its resistance with dry air.

Result and discussion

Synthesis of ZnO-OMWCNTs

The zinc oxide-oxidized multiwall carbon nanotubes (ZnO-OMWCNTs) nanocomposite was prepared via the synthetic route shown in Scheme 1. In the first step, multiwall carbon nanotubes (MWCNTs) were treated with oxidizing agents (H₂SO₄/NHO₃), leading to the oxidation and also better dispersibility/solubility of MWCNTs [4]. In the next step, OMWCNTs nanocomposites were reacted with ZnO using a simple sol–gel method based on Zhu's work [38].

The structure of the synthesized nanocomposite was fully established by different analytical techniques such as Fourier-transform infrared spectroscopy (FT-IR), X-ray diffraction (XRD), Raman spectroscopy, and scanning electron microscopy (SEM).



Scheme 1 Synthesis of zinc oxide-oxidized multiwall carbon nanotubes (ZnO-OMWCNTs)

FT-IR spectrum of MWCNTs, OMWCNTs and ZnO-OMWCNTs

Carbon nanotubes are usually in bulk form. After the functionalization of carbon nanotubes, to overcome the Van der Waals forces, they dispersed well in solution. Activated groups can play an important role in nucleation and insertion of ZnO nanoparticles [37, 39–41]. The infrared spectra of pure MWCNTs, OMWCNTs, and ZnO-OMWCNTs nanocomposite are presented in Fig. 2a–c. Figure 2a, b, respectively, shows the FT-IR spectra before and after the formation of CNT's carboxylic acid groups. The FT-IR spectra indicate the formation of carboxylic acid groups on the MWCNTs structure by appeared bands at $1000\text{--}1300\text{ cm}^{-1}$ (stretching

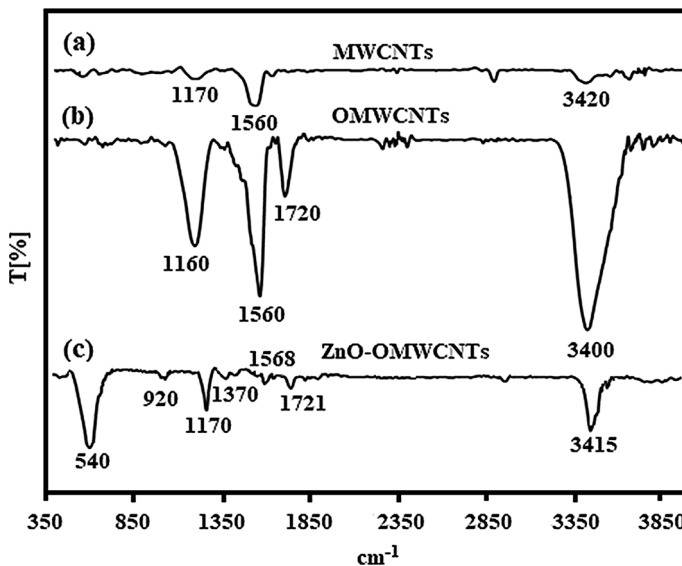


Fig. 2 FT-IR of MWCNTs (a), b OMWCNTs, and c ZnO-OMWCNTs (1 wt%) nanocomposite

bands of $\nu(\text{C}-\text{O})$) and 1720 cm^{-1} ($\text{C}=\text{O}$) and the formation of hydroxyl groups by appeared bands at 3400 cm^{-1} ($\text{O}-\text{H}$) [4]. In Fig. 2a, the absorption bands at 1170, 1560 and 1060 cm^{-1} are ascribed to inherent structure of carbon nanotubes and small peak at 3400 cm^{-1} is due to the purification process [27–29, 33, 38, 42]. As shown in Fig. 2c, the peaks at 540, 920, 1170, 1721, and 3415 cm^{-1} are related to the $\nu(\text{Zn}-\text{O})$, $\nu(\text{Zn}-\text{C})$, $\nu(\text{C}-\text{O})$, $\nu(\text{C}=\text{O})$, and $\nu(\text{O}-\text{H})$ in the ZnO-OMWCNTs nanocomposite. These results demonstrated the successful carboxylation on the wall of MWCNTs and synthesis of ZnO-OMWCNTs nanocomposite.

Structural characterizations of MWCNTs, OMWCNTs, ZnO, and ZnO-OMWCNTs (1%) nanocomposite microscopy

Analysis of scanning electron (SEM) of MWCNTs, OMWCNTs, ZnO, and ZnO-OMWCNTs (1%) nanocomposite

In this study, using electron microscopy tools, multiwall carbon nanotubes were investigated. SEM image in Fig. 3a shows the average length of MWCNTs with 5–15 μm , and external diameter of 10–20 nm. The image obtained by SEM reveals that the as-prepared OMWCNTs are distributed as spaghetti-like structures with a diameter in the range of 30 and 50 nm. SEM image in Fig. 3c shows the synthesized ZnO (by sol–gel method). The spherical morphology of the particles, pore distribution, and particle size of 27 nm is appropriate. Figure 3d, e shows the 1 wt% ZnO-OMWCNTs (Z-MW-3) nanohybrid after calcination process under argon atmosphere for 2 h. at 400 °C. As can be seen, among nanoparticles, OMWCNTs are well placed and formed the hybrid dioxide.

X-ray diffraction analysis (XRD) Nanostructured of ZnO and ZnO-OMWCNTs (1%) nanocomposite

The X-ray diffraction (XRD) patterns of ZnO and ZnO-Z-MW-3 are depicted in Fig. 4a, b. ZnO exhibits the sole main diffraction peak at $2\theta = 33.1$ (100), 36.2 (002), and 38.4° (101). Also, the additional peaks are appeared at $2\theta = 51.9$ (102), 62.8 (110), 70.5 (103), 74.9 (200), 77.1 (112), and 78.5° (201). The peaks according to JCPDS standard card number 0704-076-01 match the wurtzite hexagonal crystalline phase of ZnO. As Fig. 4 suggests, by adding 1 wt% CNT to ZnO, no change was appeared in the index peaks. A small peak at $2\theta = 26.3^\circ$ witnesses that a very low quantity of CNT was added and proves that this can be very similar in other hybrids [4, 43]. Particle size of ZnO at $2\theta = 38.5^\circ$ is 23 nm which indicates the successful formation of nano-ZnO.

Raman analysis of ZnO-OMWCNTs (1%) nanocomposite

Figure 5 indicates the Raman spectrum of ZnO-OMWCNTs (1%) nanocomposites. As shown in the Raman spectrum of ZnO-OMWCNTs, the band at 317, 430, and 550 cm^{-1} is due to mode E2 (high)-E2 (low), multiphonon of ZnO. Also, the Raman bands

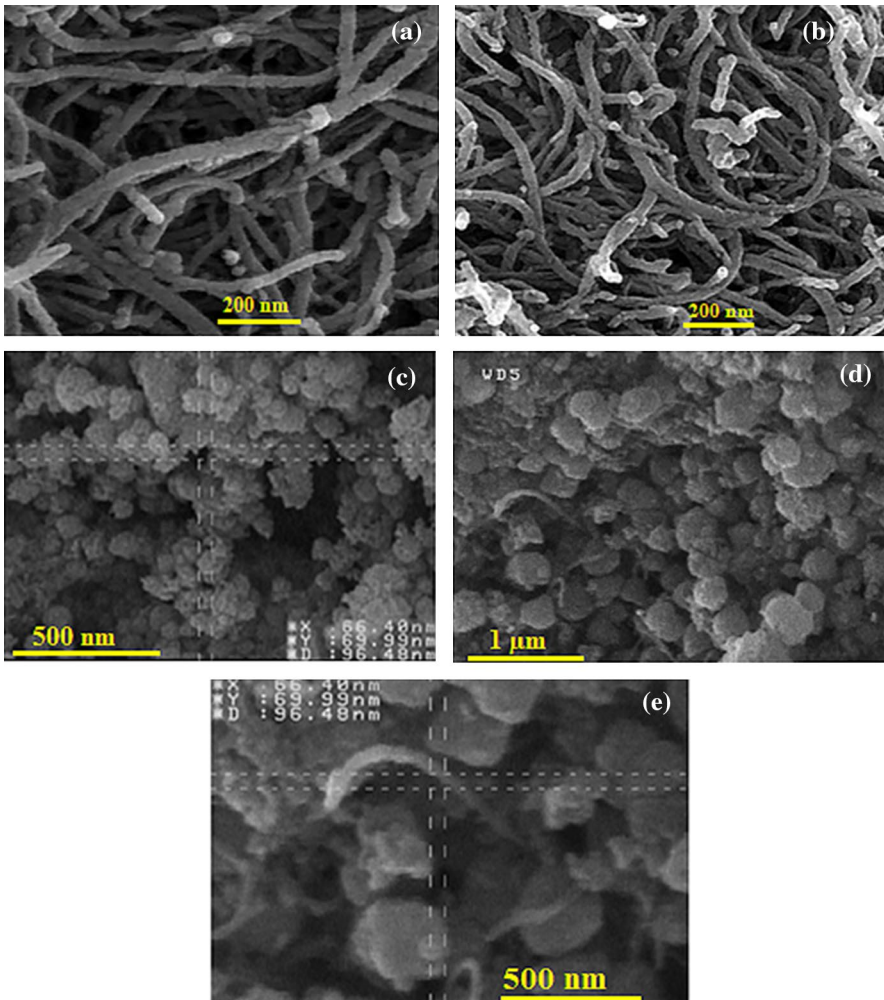


Fig. 3 SEM images of **a** MWCNTs, **b** OMWCNTs, **c** ZnO synthesized by sol-gel method, **d**, **e** ZnO-OMWCNTs (1 wt%) nanocomposite

observed at around 1095 cm^{-1} are related to the 2LO phonons of ZnO. The D and G bands of carbon OMWCNTs are assigned at about $1341, 1567\text{ cm}^{-1}$ that these results indicated the successful synthesis of ZnO-OMWCNTs nanocomposite [44].

Sensitivity

Sensor sensitivity was defined by the ratio of the changes of sensor signals to the original scope:

$$S = (\Delta R/R) \times 100 \quad (1)$$

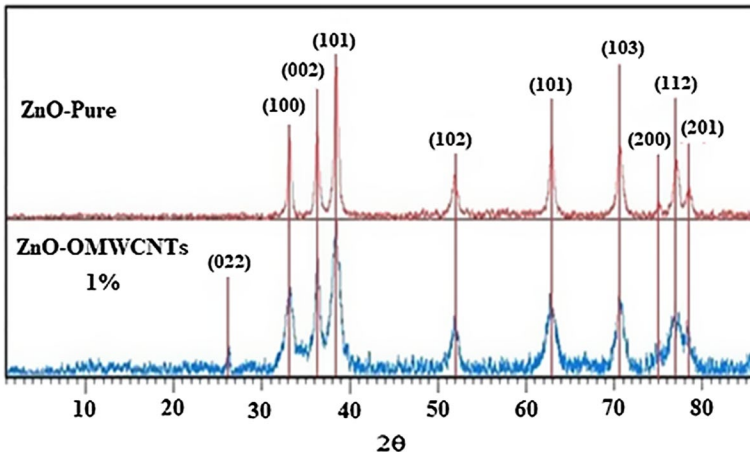


Fig. 4 X-ray diffraction pattern of a ZnO pure, and b ZnO-OMWCNTs 1%

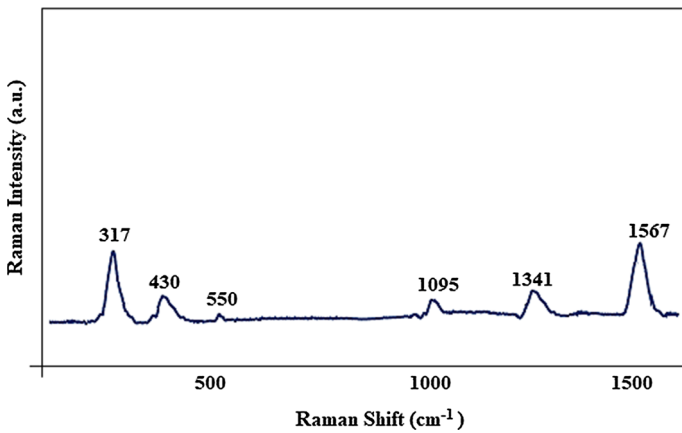


Fig. 5 Raman spectra of ZnO-OMWCNTs 1%

ΔR is the range of the sensor signal change, and R is the amplitude of the original signal. In the presence of oxidizing gas:

$$S = \frac{R_{\text{gas}} - R_{\text{air}}}{R_{\text{air}}} \tag{2}$$

R_a is the sensor resistance in dry air, and R_g is the resistance in mixture of dry air and target gas [22].

ZnO sensor

After investing, depositing and placing the sensor in the holder, the sensor was placed inside the test chamber. The air was passed from the chamber, oxygen adsorbed due to the high electronegativity, electrons removed from the conduction band, and as a result, resistance increased. After placing sensors inside the test chamber, the concentration of 20–40 ppm of NO_x gas was passed. When the oxidizing gas was adsorbed on the surface of ZnO nanostructures, oxygen atoms separated from the oxidizing gas molecules and this electron adsorbed on ZnO nanostructures. The reduction layer is thicker because of the reduced carrying loads, resulting in increased resistance [22, 23, 34]. After testing the sensors, the air was passed on it again. As shown in Fig. 6 (line a), the sensor sensitivity increases with increasing temperature to a maximum (which is said working temperature), and sensitivity decreases with increasing temperature. Working temperature in this study is 250 °C. This behavior of gases by the kinetics and mechanism of adsorption and desorption on the surface of ZnO or metal oxides have similar explanation. Sensitive sensor speeds up the chemical reactions on the surface of the seeds. Also, releasing the gas molecules depends on the sensor surface. In low temperatures, produced gas and oxygen ions remained on the surface of the sensor, so the reaction stopped on the surface. As the temperature increased, the reaction continued. By increasing the sensor temperature over its operating temperature, the kinetic energy was increased and rejection happened [16, 45].

Hybrid 0.1 wt% (Z-MW-1)

Figure 6 (line b) shows response rate for 0.1 wt% hybrid sensor by 20–40 ppm of NO_x gas. As can be seen, with the addition of CNT to ZnO, sensitivity was

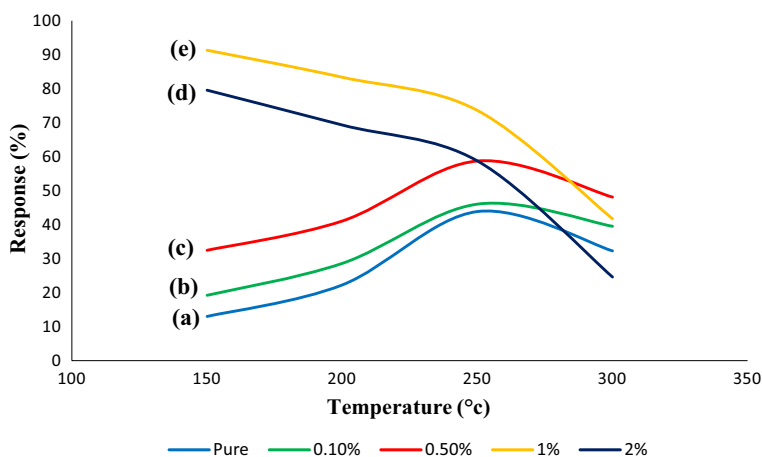


Fig. 6 Response of (line a) pure ZnO, (line b) (Z-MW-1), (line c) (Z-MW-2), (line d) (Z-MW-3), and (line e) (Z-MW-4) sensor exposed to 120 ppm NO_x gas concentration at different temperatures

increased, but by adding the low percentage of CNT to ZnO (1% by weight), these changes were not obvious [15, 19].

Hybrid 0.5 wt% (Z-MW-2)

Figure 6 (line c) indicates response rate for 0.5wt% hybrid sensor when the concentration of NO_x gas sets 20–40 ppm. As can be seen, with the addition of CNT to 0.5 wt% of ZnO, sensitivity was increased (in comparison with 0.1 wt% of ZnO). Furthermore, adding carbon nanotube to the metal oxide leads to more increased response [18, 19].

Hybrid 1 wt% (Z-MW-3)

Figure 6 (line d) shows response rate for 1 wt% hybrid sensor by 20–40 ppm of NO_x gas. As expected, with the addition of 1% CNT, responsiveness was increased. As temperatures rises, the response rate of sensor was decreased. This result is due to the addition of too much of CNT. By exceeding the temperature from a certain limit, resistance was decreased significantly (by connecting CNTs) and leads to a shorter resistive route in sensors which affected the process. By adding carbon nanotubes, sensitivity was increased. But sensitivity of the ZnO-OMWCNTs composite by increasing the amount of carbon nanotubes was reduced. Therefore, to obtain an ideal sensor, presence of optimized amount of carbon nanotubes is very important. When temperature was increased to above 150 °C, response rate of sensor has weakened. This declining trend is more noticeable than other weight percentages which could be due to changes in hybrid properties at higher temperatures (due to the presence of more CNT, its burning, and adverse effects on ZnO behavioral characteristics) [15, 20, 46].

Hybrid 2 wt% by weight (Z-MW4)

Figure 6 (line e) shows response rate for 2 wt% hybrid sensor by 20–40 ppm of NO_x gas. By adding 2 wt% of CNT, response was decreased in comparison with 1 wt% of CNT. This is due to the change in hybrid properties at higher temperatures. This means that at low temperatures, the electrical properties of the CNT increase the response. However, at higher temperatures, the optimal effect of increasing the percentage of CNT decreases and the behavior of the material tends to change ZnO [15, 39, 40, 46–48].

Recovery times

An ideal sensor addition (for high sensitivity) must have an optimum recovery time. The high response time or not optimized recovery time cannot lead to a high sensor sensitivity sensor.

Recovery time at 150 °C

The recovery times of different samples of NO_x sensor (20 ppm concentration of NO_x gas) are presented in Fig. 7 at different temperatures. According to Fig. 7 at 150 °C, the minimum recovery time is related to sample (Z-MW-3). By increasing the response rate, recovery time was decreased [39, 40]. This is also true for other synthesized hybrids.

Recovery time at 200 °C

As shown in Fig. 7, with an increase in the response, recovery time was reduced. Z-MW-3 sensor has the shortest recovery time among other sensors. With the increase in the operating temperature and the conductivity of the material, the recovery time was decreased. This result is consistent with all rules about semiconductor sensors [21, 49, 50].

Recovery time at 250 °C

At this temperature, it can be seen that by increasing the operational temperature, the recovery time was reduced. Figure 7 shows recovery time at 250 °C [21, 50, 51].

Recovery time at 300 °C

According to Fig. 7, the expected recovery time was increased. With the increase in temperature over operating temperature, the material lost its structural features and sensor sensitivity was reduced. These results indicated that response time increased [25, 49–52]. Generally, with increasing temperature and also increasing the amount of CNT in the composites, the response time decreased. It is clear that in the sample containing 2% CNT and 20 ppm of the target gas, the detection

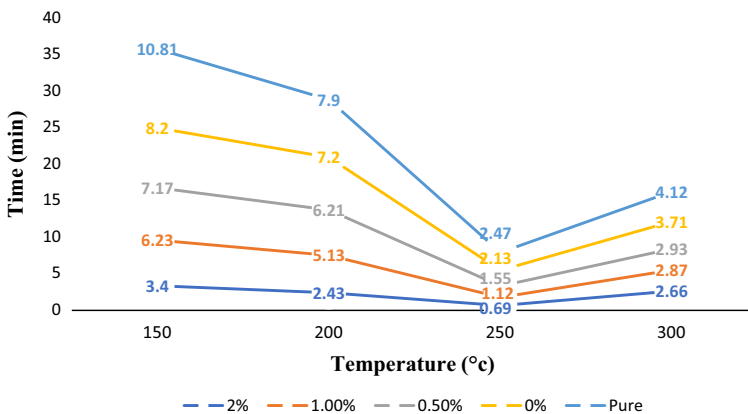


Fig. 7 Recovery times of different sensors at temperatures (150, 200, 250, and 300 °C)

time was 0.69 min, but with increasing temperature and at 250 °C, the response time was increased again.

Gas sensing and repeatability performances of ZnO-OMWCNTs sensor (20–40 ppm concentration of NO_x gas) at different temperature are indicated in Fig. 8. As can be seen in Fig. 8, by repeatedly injecting the gas to the system, the sensor's resistance increased and decreased intermittently. This indicates the sensor's sensitivity to NO_x gas, and also its repeatability during successive tests. By trapping electrons from the conduction band on the surface of the sample into different ions, the oxygen molecules are chemically adsorbed (in the presence of air). This action increases the potential barrier and the resistance. By exposing the sensor to the NO_2 , the gas is chemically adsorbed and reacted with oxygen ions, and the trapped electrons return to the conduction band, finally resulting in decreased resistance and increased conductivity.

A comparison between gained results of the present work and previous studies can be seen in Table 2. ZnO-OMWCNTs (0.1 wt%) gas sensor indicated best performance in low detection range of NO_x -sensor (20–40 ppm of NO_x gas concentration) and optimized temperature (at 250 °C). However, because of the differences in experimental conditions, comparison between these studies must be done with caution.

The most important and plausible mechanisms that can be explained for ZnO-OMWCNTs NO_x gas sensor and NO_x (NO/NO_2) are illustrated in Scheme 2. ZnO metal oxide is an n-type semiconductor and acts as an electron donor group by having a free electron. Also, NO_x gas acts as an electron-accepting group that adsorbed on the surface of nanocomposite and changed to NO^- and NO_2^- ions. Additionally, carbon nanotubes are p-type semiconductors that increase the interaction between the gas molecules and the nanocomposite surface [56–58].

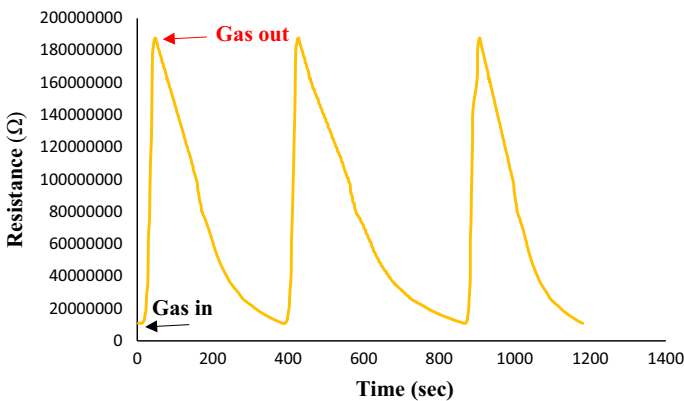
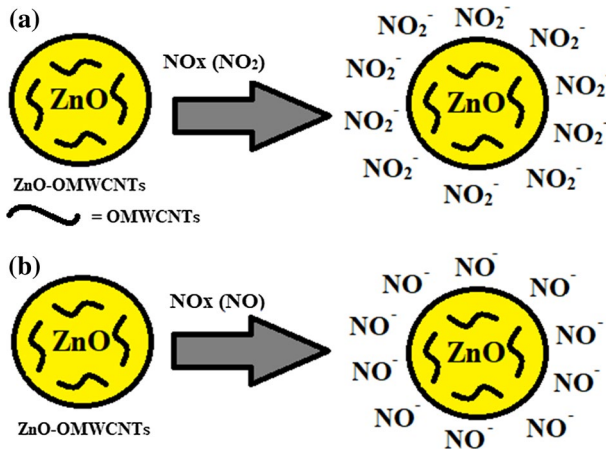


Fig. 8 Sensor resistance changes during three repetitions of the test against the target gas

Table 2 Comparison of NO_x-sensor capacity from the present study with those reported for other materials used in laboratory-scale NO_x-sensing processes

Metal oxide	Dopant optimal concentration	Morphology	Method	Optimal temperature (°C)	Detection range (ppm)	Response/ ppm		Response time (s)	References
						S	C		
ZnO	MWCNT (1 wt%)	Composite	Sol-gel/spin coating	250	20–40	58	40/60	235	Present work
ITO	SnO ₂ (15%)	Thin film	RF magnetron sputtering	327	5–200	27	50	–	[51]
In ₂ O ₃	WO ₃ (3–5 mol%)	Tick films	Commercial	250	4–50	4.71/122	4/50	420–540	[53]
In ₂ O ₃	Cd ₂ O ₃ (3–5 mol%)	Tick films	Commercial	250	4–50	5.84/51.3	4.50	15–20	[53]
SnO ₂ -WO ₃	Zn (3 wt%)	Composite	Sol precipitation	200	0.01–40	250	200	–	[44]
ZnO-SnO ₂	Pt (1 wt%)	Composite	Reverse micro-emulsion	200	200–1000	29.6	600	500	[54]
ZnO-SnO ₂	Pd (1 wt%)	Composite	Reverse micro-emulsion	200	200–1000	69.7	500	500	[54]
ZnO	–	Pencil-like nanorods	Hydrothermal	400	40	224	40	–	[16]
SnO ₂	–	Nanowires	Thermal evaporation	300	0.5–100	5	1	35	[55]



Scheme 2 Schematic illustration of the NO_x gas (NO/NO_2) sensing mechanism for zinc oxide-oxidized multiwall carbon nanotubes (ZnO-OMWCNTs) gas sensor and transfer to **a** NO_2^- , **b** NO^-

Conclusion

In this study, the properties of pure ZnO sensor and a hybrid of 0.1 wt%, 0.5 wt%, 1 wt%, and 2 wt% OMWCNTs verified and evaluated in order to detect NO_x gas. Concentration of about 20–40 ppm was chosen for the target gas. The structure of this newly synthesized ZnO-OMWCNTs nanocomposite was fully characterized by X-ray diffraction (XRD), scanning electron microscopy (SEM), and Fourier-transform infrared (FT-IR) techniques, and it was found that the addition of OMWCNTs to ZnO can be made high sensitivity sensors. The high surface area and unique electronic properties of MWCNTs lead to improving the performance of metal oxides. Pure ZnO nanohybrids containing OMWCNTs have a higher surface area (as a result of more gas adsorption), faster and shorter response time. Sensor test results indicate that the best nanocomposite is containing 1 wt% of OMWCNTs (Z-MW-3). This nanocomposite is about 7 times more sensitive than pure ZnO at 150 °C. This sensitivity is due to improved properties of ZnO. Detection of NO_x gas by ZnO-OMWCNTs was studied under different experimental conditions, and the results were compared with those obtained with ZnO and another metal oxide. The results show that the responsiveness, detection range, and optimum temperature of present work are improved compared to other work.

Acknowledgements The authors wish to thank the Research Council of Semnan University for financial support to carry out this research. The Research Institute of Petroleum Industry (RIPI) is also greatly acknowledged for technical support.

References

1. W. Tsujita, A. Yoshino, H. Ishida, T. Moriizumi, *Sens. Actuators B*, **110**, 304 (2005)
2. O. pummakarnchana, N. Tripathi, J. Dutta, *Sci. Technol. Adv. Mater.* **6**, 251 (2005)
3. J. Robert. Blaszczcka, [www3. Epa .gov](http://www3.epa.gov), U.S. EPA, RTP, NC 27711–2012
4. A. Rashidi, M.K. Abbasabadi, S. Khodabakhshi, *J. Nat. Gas Sci. Eng.* **36**, 13 (2016)
5. A. Rashidi, Z. Tavakoli, Y. Tarak, S. Khodabakhshi, M.K. Abbasabadi, *J. Chin. Chem. Soc.* **63**, 399 (2016)
6. M.K. Abbasabadi, A. Rashidi, J. Safaei-Ghomi, S. Khodabakhshi, R. Rahighi, *J. Sulfur Chem.* **36**, 660 (2015)
7. M.K. Abbasabadi, A. Rashidi, S. Khodabakhshi, *J. Nat. Gas Sci. Eng.* **28**, 87 (2016)
8. D. Azarifar, M. Khaleghi-Abbasabadi, *Res. Chem. Intermed.* **45**, 2095 (2019)
9. S. Khodabakhshi, F. Marahel, A. Rashidi, M.K. Abbasabadi, *J. Chin. Chem. Soc.* **62**, 389 (2015)
10. D. Azarifar, M. Khaleghi-Abbasabadi, *Res. Chem. Intermed.* **45**, 199 (2019)
11. S. Khodabakhshi, P.F. Fulvio, E. Andreoli, *Carbon* **162**, 604 (2020)
12. N. Esmaili, J. Rakhtshah, E. Kolvari, H. Shirkhanloo, *Microchem. J.* **154**, 104632 (2020)
13. H. Shirkhanloo, K. Merchant, M.D. Mobarake, *J. Anal. Chem.* **74**, 865 (2019)
14. T. Hashishin, J. Tamaki, *Sens. Mater.* **21**, 265 (2009)
15. P.G. Collins, K. Bradley, M. Ishigami, A. Zettl, *Science* **287**, 1801 (2000)
16. B.Y. Wei, M.C. Hsu, P.G. Su, H.M. Lin, R.J. Wu, H.J. Lai, *Sens. Actuators B Chem.* **101**, 81 (2004)
17. M. Ahmad, E. Ahmed, Z.L. Hong, W. Ahmed, A. Elhissi, N.R. Khalid, *Ultrason Sonochem.* **21**, 761 (2014)
18. B. Shoulia, C. Liangyuanb, L. Dianqinga, Y. Wenshenga, Y. Pengchenga, L. Zhiyonga, C. Aifana, C.C. Liub, *Sens. Actuators B* **146**, 129 (2010)
19. S. Khodabakhshi, M.K. Abbasabadi, S. Heydarian, S.G. Shirazi, F. Marahel, *Lett. Org. Chem.* **12**, 465 (2015)
20. S. Dastkhoon, Z. Tavakoli, S. Khodabakhshi, M. Baghernejad, M.K. Abbasabadi, *New J. Chem.* **39**, 7268 (2015)
21. I. Sayago, H. Santos, M.C. Horrillo, M. Aleixandre, M.J. Fernandez, E. Terrado, I. Tacchini, R. Aroz, W.K. Maser, A.M. Benito, M.T. Martinez, J. Gutierrez, E. Munoz, *Talanta* **77**, 758 (2008)
22. S.W. Choi, J.Y. Park, S.S. Kim, *Nanotechnology* **20**, 465603 (2009)
23. R. Kumar, O. Al-Dossary, G. Kumar, A. Umar, *Nano-Micro Lett.* **7**, 97 (2015)
24. A. Wei, L. Pan, W. Huang, *Mater. Sci. Eng. B Adv.* **176**, 1409 (2011)
25. C. Zhang, M. Debliquy, H. Liao, *Appl. Surf. Sci.* **256**, 5905 (2010)
26. M. Breedon, M.J.S. Spencer, I. Yarovsky, *J. Phys. Chem.* **114**, 16603 (2010)
27. A. Begum, K.M. Tripathi, S. Sarkar, *Chem. Eur. J.* **20**, 1 (2014)
28. K.M. Tripathi, A. Begum, S.K. Sonkara, S. Sarkar, *New J. Chem.* **37**, 2708 (2013)
29. G.S. Das, S. Sarkar, R. Aggarwal, S.K. Sonkar, J.-W. Park, K.M. Tripathi, T.Y. Kim, *Carbon Lett.* **29**, 595 (2019)
30. H. Shan, C. Liu, L. Liu, L. Wang, X. Zhang, X. Chi, X. Bo, K. Wang, *Chin. Sci. Bull.* **59**, 374 (2014)
31. K.Y. Choi, J.S. Park, K.B. Park, H.J. Kim, H.D. Park, S.D. Kim, *Sens. Actuators B Chem.* **150**, 65 (2010)
32. E.H. Espinosa, R. Ionescu, B. Chambon, G. Bedis, E. Sotter, C. Bittencourt et al., *Sens. Actuators B Chem.* **127**, 137 (2007)
33. A. Wisitsoraat, A. Tuantranont, C. Thanachayanont, V. Patthanasettakul, P. Sing-jai, *J. Electroceram.* **17**, 45 (2006)
34. C. Sun, G. Maduraiveeran, P. Dutta, *Sens. Actuators B Chem.* **186**, 117 (2013)
35. R. Lotfi, A.M. Rashidi, A. Amrollahi, *Int. Commun.* **39**, 108 (2012)
36. A.M. Rashidi, M. Mirzaeian, S. Khodabakhshi, *J. Nat. Gas Sci. Eng.* **25**, 103 (2015)
37. R. Yudianti, H. Ongo, Sudirman, Y. Saito, T. Iwata, J.I. Azuma, *Science and engineering.* **35**, 37 (2010)
38. L.P. Zhu, G.H. Liao, W.Y. Huang, L.L. Mac, Y. Yang, Y. Yu, S.Y. Fu, *Mater. Sci. Eng. B* **163**, 194 (2009)
39. C. Balazsi, K. Sedlackova, E. Llobet, R. Ionescu, *Sens. Actuators B Chem.* **133**, 151 (2008)
40. M.K. Ram, O. Yavuz, M. Aldissi, *Synth. Met.* **151**, 77 (2005)

41. J.H. Lee, J. Kim, H.W. Seo, J.W. Song, E.S. Lee, M. Won, C.S. Han, *Sens. Actuators B Chem.* **129**, 628 (2008)
42. S. Demoustier, E. Minoux, M. Le Baillif, M. Charles, A. Ziaei, *C R Phys.* **9**, 53 (2008)
43. H.F. McMurdie, M.C. Morris, E.H. Evans, B. Paretzkin, W. Wong-Ng, L. Ettliger, C.R. Hubbard, *Powder Diffr.* **1**, 64 (1986)
44. G. García-Valdivieso, J.J. Velázquez-Salazar, J.E. Samaniego-Benítez, H.J. Ojeda-Galván, M.J. Arellano-Jiménez, K.G.H. Martínez-Reyna, M. José-Yacamán, H.R. Navarro-Contreras, *Nanotechnology* **29**, 125607 (2018)
45. B. Shouli, L. Dianqing, H. Dongmei, L. Ruixian, C. Aifan, C.C. Liu, *Sens. Actuators B Chem.* **150**, 749 (2010)
46. N.D. Hoa, N.V. Quy, D. Kim, *Sens. Actuators B Chem.* **142**, 253 (2009)
47. R. Leghrib, R. Pavelko, A. Felten, A. Vasiliev, C. Cane, I. Gracia, J.J. Pireaus, E. Llobet, *Sens. Actuators B Chem.* **145**, 411 (2010)
48. W.D. Zhang, B. Xu, L.C. Jiang, *J. Mater. Chem.* **20**, 6383 (2010)
49. Y. Qin, M. Hu, J. Zhang, *Sens. Actuators B Chem.* **150**, 339 (2010)
50. L. Wei, H. Shizhen, C. Wenzhe, *J. Semicond.* **31**, 024006 (2010)
51. M. Breedon, P. Spizziri, M. Taylor, J.D. Plessis, D. McCulloch, J. Zhu, L. Yu, Z. Hu, C. Rix, W. Wlodarski, K. Kalanter-Zadeh, *Cryst. Growth Des.* **10**, 430 (2010)
52. R.K. Joshi, H. Gomez, F. Alvi, A. Kumar, *J. Phys. Chem.* **114**, 6610 (2010)
53. K. Vijayalakshmi, C. Ravidhas, V.V. Pillay, D. Gopalakrishna, *Thin Solid Films* **519**, 3378 (2011)
54. T.V. Belysheva, L.P. Bogovtseva, E.A. Kazachkov, N.V. Serebryakova, *J. Anal. Chem.* **58**, 646 (2003)
55. C. Liangyuan, B. Shouli, Z. Guokun, L. Dianqing, C. Aifan, C.C. Liu, *Sens. Actuators B Chem.* **134**, 360 (2008)
56. B.A. Albiss, W.A. Sakhaneh, I. Jumah, I.M. Obaidat, *IEEE Sens. J.* **10**, 1807 (2010)
57. Z. Wang, Z. Xie, L. Bian, W. Li, X. Zhou, X. Wu, Z. Yang, N. Han, J. Zhang, Y. Chen, *Mater. Sci. Appl.* **215**, 1700861 (2018)
58. B.G. Kim, D.G. Lim, J.H. Park, Y.J. Choi, J.G. Park, *Appl. Surf. Sci.* **257**, 4715 (2011)

Publisher's Note Springer Nature remains neutral with regard to jurisdictional claims in published maps and institutional affiliations.